ELSEVIER

Journal of Nuclear Materials 296 (2001) 203–209

journal of nuclear materials

www.elsevier.com/locate/jnucmat

Ion-irradiation-induced hardening in Inconel 718

J.D. Hunn *, E.H. Lee, T.S. Byun, L.K. Mansur

Metals and Ceramics Division, Oak Ridge National Laboratory, P.O. Box 2008, Oak Ridge, TN 37831-6151, USA

Abstract

Inconel 718 is a material under consideration for areas in the target region of the spallation neutron source (SNS), now under construction at Oak Ridge National Laboratory (ORNL) in the US. In these positions, displacement damage from protons and neutrons will affect the mechanical properties. In addition, significant amounts of helium and hydrogen will build up in the material due to transmutation reactions. Nanoindentation measurements of solution-annealed (SA) Inconel 718 specimens, implanted with Fe-, He-, and H-ions to simulate SNS target radiation conditions, have shown that hardening occurs due to ion-induced displacement damage as well as due to the build-up of helium bubbles in the irradiated layer. Precipitation-hardened (PH) Inconel 718 also exhibited hardening by helium build-up but showed softening as a function of displacement damage due to dissolution of the γ' and γ'' precipitates. Published by Elsevier Science B.V.

PACS: 61.82.Bg; 61.80.Jh

1. Introduction

The spallation neutron source (SNS) will utilize a 1 GeV proton beam incident on a metal target vessel containing liquid mercury for cooling and neutron production. Notable radiation effects will include radiation-induced displacement damage, from both incident protons and spallation neutrons, and the creation of transmutation products, especially hydrogen (up to 1000 appm/dpa) and helium (up to 200 appm/dpa). As part of the materials R&D effort for this project, spallation radiation effects are being studied by using a unique triple-ion facility (TIF) at Oak Ridge National Laboratory (ORNL). For these experiments, specimens have been bombarded by 3500 keV Fe-ions in order to simulate the displacement damage expected from the proton and neutron fluxes in the SNS target. Simultaneously, He- and H-ions were injected at energies calculated to overlap the Fe-induced damage profile. To further elucidate the individual contributions of displacement damage and trapped gas, specimens were also irradiated by Fe- and He-ions alone [1]. In addition, hydrogen retention has been studied previously and found to be significant in steels containing trapped helium [2]. To date, specimens studied include 316LN stainless steel [1–5], a 9Cr–2WVTa ferritic/martensitic steel [6], and Inconel 718 [this paper]. 316LN is the current design material for the SNS mercury vessel. Inconel 718 has been in use at the LANSCE facility at Los Alamos National Laboratory for accelerator vacuum windows and various other components, and is a candidate material for the SNS accelerator vacuum window and a back-up candidate for the mercury vessel.

2. Experimental

Three millimeter diameter disks of Inconel 718 were prepared by punching from a 0.25 mm thick rolled sheet. After final polishing with 0.1 μm diamond paste, specimens were solution-annealed (SA) at 1065°C for 30 min. Some specimens were also hardened by thermal aging at 750°C for 10 h followed by 650°C for 20 h. This thermal aging resulted in the formation of γ' and γ'' precipitates. After annealing, specimens were electropolished to expose a virgin surface. Irradiations were carried out at ORNLs TIF [7]. The specimens were heated to 200°C

* Corresponding author. Tel.: +1-865 574 2480; fax: +1-865 574 0641.

E-mail address: hunnjd@ornl.gov (J.D. Hunn).

0022-3115/01/$ - see front matter. Published by Elsevier Science B.V.
PII: S0022-3115(01)00519-0

during irradiation and the three ion beams were defocused to provide a uniform ion flux across the entire surface area. H-ions were incident along the normal to the surface, while Fe and He were injected at 15° off normal, as dictated by the TIF beam-line geometry. Fluence was monitored for all three beams and ion fluxes were controlled during multiple ion irradiations to maintain the appropriate appm to dpa ratio.

Ion energies were chosen to overlap the injected He and H profiles with the peak in the Fe-induced displacement profile at a depth of around 825 nm (see Fig. 1). This depth was sufficient to avoid surface effects on the damage accumulation in this region [8,9]. The computer program SRIM-2000 [10], with a modified Kinchen–Pease approximation, was used to calculate these profiles. Table 1 lists the values calculated by SRIM for the three implanted species. The average concentrations about the 825 nm peak for the He and H injections were calculated as the mean between the two half-maximum points given in the table for each profile. These numbers were then used to calculate the appropriate ion fluences to give approximately 200 appm He/dpa and 1000 appm H/dpa in the region about 825 nm. The initial damage distribution from the Fe-irradiation was calculated in terms of dpa (displacements per atom) using the NRT formula [11]

$$\mathrm{dpa} = \frac{0.8}{2E_\mathrm{d}}\left(\frac{\mathrm{d}E}{\mathrm{d}x}\right)_n \frac{\phi_t}{\rho}, \tag{1}$$

where ϕ_t was the ion fluence, ρ was the atomic density, $E_\mathrm{d} = 40$ eV was the displacement energy, and $(\mathrm{d}E/\mathrm{d}x)_n$ was the linear energy transferred (LET) per ion to the target by nuclear processes. $(\mathrm{d}E/\mathrm{d}x)_n$ was obtained from SRIM by summing the phonon and binding energy distribution profiles. The binding energy profile was obtained from the vacancy profile output by SRIM multiplied by the binding energy used for the calculation. The average dpa about 825 nm, used to calculate the appropriate Fe-ion fluence, was taken as the mean between 700 and 930 nm. This was essentially the same region used to average the He profile and was also the layer later analyzed by transmission electron microscopy (TEM). The additional dpa introduced by the helium and hydrogen in the triple-beam irradiations was negligible (<2%). In the following results and discussion the reported displacement doses and helium concentrations are the average values in the region centered around 825 nm depth, as calculated from Table 1.

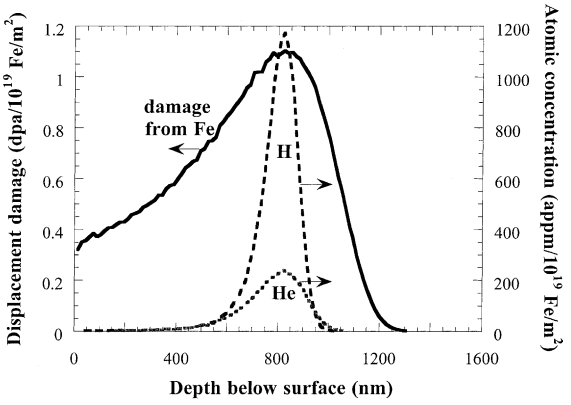

Fig. 1. SRIM simulation of the initial displacement profile from 3500 keV Fe-ions and the initial helium and hydrogen profiles, before diffusion, for 370 keV He- and 180 keV H-implantation.

Previous studies have found that the final He profile can be expected to be essentially the same as the calculated initial profile due to the very low solubility and high detrapping energy for He in this type of alloy at this temperature [12–15]. Nuclear reaction analysis measurements of specimens implanted with Fe, He, and D under similar conditions suggest that the final H profile will duplicate the He profile due to trapping of the hydrogen around the helium, but with only a few percent of the injected hydrogen retained at 200°C [2].

Ion fluxes were varied depending on the desired fluence, a practical necessity to allow irradiations to be performed in a reasonable time period, since the fluences ranged over several orders of magnitude. Damage rates from the Fe-irradiation were from 10^{-4} to 3×10^{-3} dpa/s, with associated gas injection rates of 0.02–0.6 appm He/s and 0.1–3 appm H/s. He-injection rates for the higher concentration He-only implants went as high as 2 appm/s. The SNS will operate with an average dose rate of 10^{-6} dpa/s, in a pulsed mode with a damage flux

Table 1
Irradiation depth profiles for Inconel 718 were calculated by SRIM [10][a]

Ion energy and species	Position of peak (nm)	Position of half-max in profile relative to peak (nm)	Average concentration (per 10^{19} ions/cm^2)
180 keV H	826	−80, +60	564 appm
370 keV He[b]	826	−135, +100	350 appm
3500 keV Fe[b]	830	−530, +230	1.1 dpa

[a] Non-symmetric 'half' widths about the peaks reflect a skewing toward the irradiated surface. Average concentrations were calculated as described in the text. Energies were chosen such that the He- and H-ions profiles overlapped the Fe-induced displacement profile (Fig. 1).

[b] He and Fe profiles were calculated for 15° off of normal to reflect TIF configuration.

during the pulse of around 10^{-2} dpa/s and corresponding transmutation rates up to 2 appm He/s and 10 appm H/s. The ion fluxes were lower than this SNS beam-on rate, however, in this recombination dominant regime of high dose rate and low temperature, we expect irradiation variable shifts [16] to be minimal.

The relative effect of the various irradiations on hardening of the implanted layer was measured by a nanoindentation technique. Nano Instrument's nanoindenter II was used in the continuous stiffness mode to measure the hardness as a function of depth [17]. For these tests, the Berkovich diamond indenter tip sampled the hardness in the region of the indent and extending down about seven times the indenter's contact depth [18]. A contact depth of 150 nm was used in comparing the relative hardness as a function of irradiation dose. This depth gave a good sampling of the irradiation-induced hardening in the first micron of material. For contact depths smaller than 100 nm, the measured hardness values were subject to surface effects and uncertainty in the indenter geometry, and for values greater than 200 nm, the indenter started sampling more and more of the unimplanted material below the 1 μm thick implanted layer. It should be noted that the nanoindenter could not provide a measurement of the 'true' hardness at each depth because it was sampling a volume over which the hardness varied as a function of depth. Nevertheless it was possible to make comparisons of the relative hardening effect as a function of dose for the different irradiations and use this information to understand hardening trends.

Data appearing in the figures typically came from the averaging of 15 indents performed on separate grains from 3 separate specimens, implanted under identical conditions. For each indent, typical deviation from the mean was less than 0.1–0.2 GPa. Visual inspection during selection of the position for each indent was used to avoid obvious surface defects. Occasional anomalous indents yielding oddly shaped depth profiles or hardness values well outside the typical variation from the mean were discarded before averaging.

Specimens were prepared for examination of microstructure by TEM by first carefully electropolishing away the first 700 nm from the surface. The specimens were then backthinned until perforation occurred and analyzed around the hole at about 100 nm thickness using a Philips CM-12 at 120 keV. Some TEM results are discussed in this paper, more will appear in a later report.

3. Results and discussion

3.1. Solution-annealed Inconel 718

Fig. 2 shows the near surface hardness, as measured by the nanoindenter, as a function of the contact depth

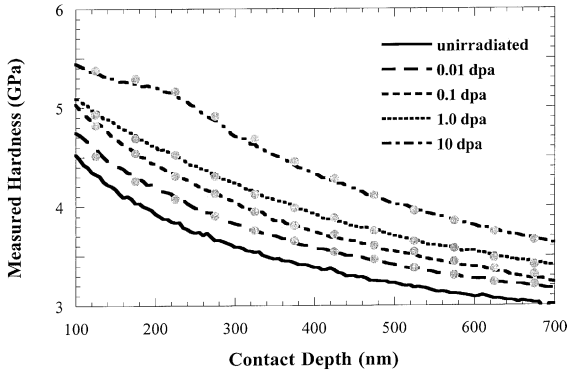

Fig. 2. Hardness as a function of contact depth, as measured by the nanoindentation technique, for SA Inconel 718 specimens irradiated with Fe-, He- and H-ions. The solid circles are selected data points from hardness profiles for similar irradiations with Fe-only. The Fe-only data overlaps the triple-beam results for each dose.

of the indenter tip for SA Inconel 718 specimens irradiated to various dpa. A systematic radiation-induced hardening was clearly evident. This hardening was similar to what had been observed previously in 316LN austenitic [3,4] and 9Cr–2WVTa ferritic/martensitic [6] alloys. It was associated with the production of 'black dot' defects (small vacancy and interstitial clusters), which appeared at very low dose and increased in density up to about 1 dpa. At higher dose, faulted and unfaulted Frank-type loops evolved and continued to produce hardening at a slower rate. Plotted in Fig. 2 are the results for both triple-beam irradiation (the lines) and specimens irradiated to an equivalent dose with Fe-ions alone (the data points overlaying each line). Up to 10 dpa, no measurable difference in hardening was observed due to the co-injection of helium and hydrogen. However, 10 dpa corresponded to only 0.2 at.% He at the 200 appm/dpa ratio used for the triple-beam irradiation.

In order to investigate the possible role of trapped gas in the observed hardening, helium was implanted by itself and to higher concentrations. Fig. 3 shows the effect of helium injection on the near surface hardening for SA Inconel 718 specimens implanted with He-ions alone. Hardening increased as a function of the concentration of trapped helium from 0.02 to 20 at.% He. This also replicated the behavior observed in 316LN stainless steel [1]. As was true in that case, the amount of hardening observed for the helium-injected specimens could not be explained by displacement damage alone. Fig. 4 compares the percent hardening, relative to an unirradiated specimen, measured by the nanoindenter at 150 nm contact depth for specimens irradiated by Fe-ions versus He-ions. Fe-ions were initially more effective in creating deformation inhibiting defects for the same

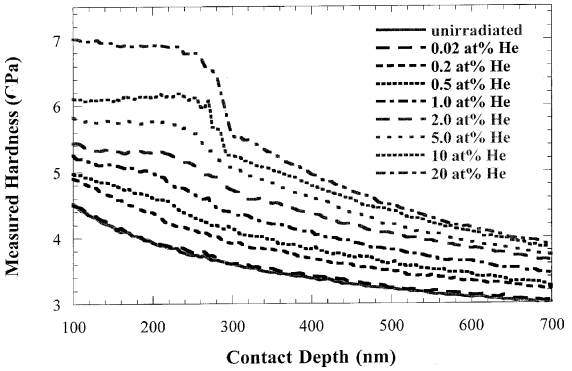

Fig. 3. Hardness as a function of contact depth for SA Inconel 718 specimens irradiated with He-ions to various concentration.

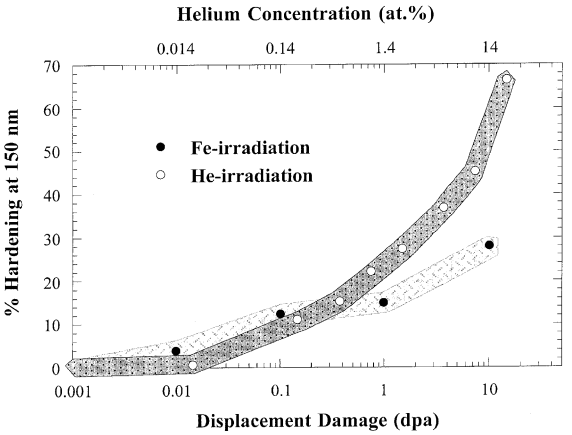

Fig. 4. Percent hardening at 150 nm contact depth, relative to the unirradiated material, for SA Inconel as a function of displacement damage from 3500 keV Fe-ions and 370 keV He-ions. Upper axis shows the associated helium concentration for the He-irradiation (open circles).

number of displacements. In TEM studies of the microstructure of 316LN irradiated under similar conditions [5], it was observed that black dot evolution and loop growth were slower as a function of dpa for He-irradiation compared to Fe-irradiation. This was attributed to several factors, including the slower damage rate and lower cascade energy for the He-irradiation. However, above a concentration of 1 at.% He, the hardening in the He-implanted Inconel was measured to be greater than that observed stemming from the Fe-induced displacement damage. This effect, also seen in 316LN, was found to be accompanied by the production of observable helium bubbles in the implanted layer [5]. Once formed, the helium bubbles presented a greater barrier to dislocation motion than the black dot and Frank loop defects.

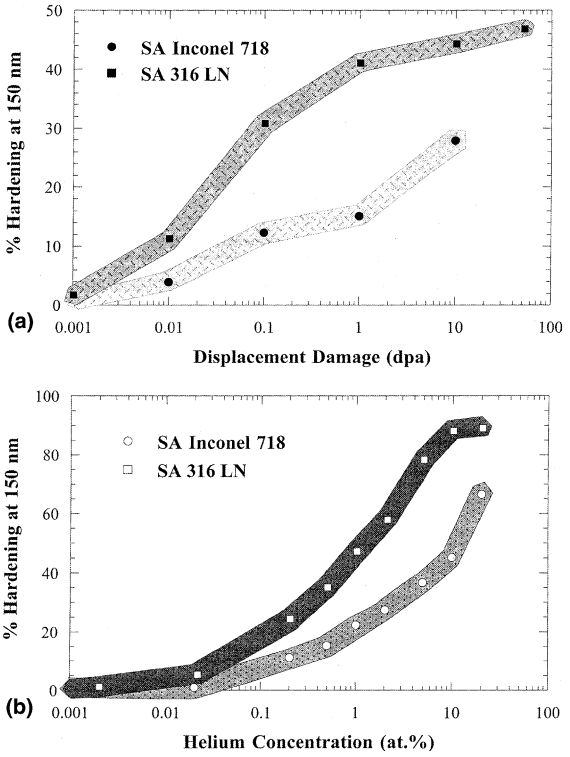

Fig. 5. Comparison of percent hardening in SA Inconel 718 and SA 316LN stainless steel as a function of (a) displacement damage from 3500 keV Fe-irradiation and (b) helium concentration from 370 keV He-injection (360 keV for the 316LN).

At 150 nm contact depth, the unirradiated SA Inconel 718 measured 44% harder than the virgin 316LN, and remained harder under identical irradiation conditions. However, Fig. 5 compares the relative hardening caused by Fe- and He-irradiation for SA Inconel 718 and 316LN stainless steel. Irradiation-induced hardening appeared to occur more rapidly, as a function of displacement damage, in the 316LN alloy. In addition, a saturation in hardening had been reached in the stainless steel that was not evident for the Inconel up to the maximum implant doses obtained in this test. This may be due to the compositional differences between the two materials, which could produce a difference in radiation-induced microstructural evolution, leading to this observed difference in hardening rate. Further study is needed.

3.2. Precipitation-hardened Inconel 718

A second set of specimens was prepared in the precipitation-hardened (PH) condition by thermal aging as described above. In the unirradiated state, the PH material was considerably harder than its SA counterpart, as expected due to the high density of γ' and γ'' precip-

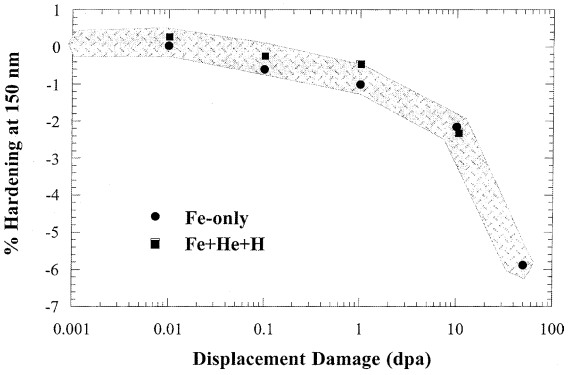

Fig. 6. Percent hardening at 150 nm contact depth, relative to the unirradiated material, for PH Inconel as a function of displacement damage from Fe-only and from triple-beam irradiation.

itates. The nanoindentation technique gave a measured hardness value at 150 nm contact depth of 4.2 GPa for the SA Inconel and 6.3 GPa for the PH Inconel. Thus the unirradiated PH Inconel 718 was still harder than the SA Inconel after 10 dpa of irradiation with Fe-ions.

In contrast to the SA specimens, displacement damage in the PH material produced a net softening effect. This is illustrated by Fig. 6, which shows a systematic reduction in the measured hardness at 150 nm contact depth. The measured effect was small, but still within the resolution of the technique. As in the SA material, the triple-beam irradiation showed essentially the same result as for specimens irradiated with Fe-ions alone. Similar softening has been observed in specimens irradiated by 800 MeV protons [19,20] and 5 MeV Ni-ions [21].

TEM analysis of the irradiated layer identified the cause of softening to be the dissolution of the γ' and γ'' precipitates, in agreement with findings from 800 MeV proton irradiations [20,22]. Even though the Fe-ion irradiation also introduced radiation defects, the loss of the precipitates outweighed the hardening contribution from these defects. This might be expected from a comparison of the relative hardness of the unirradiated PH material and the Fe-irradiated SA Inconel.

Figs. 7 and 8 show the microstructures and diffraction patterns as a function of dose for Fe-irradiated PH Inconel 718. Figs. 7(a) and 8(a) clearly show the precipitates and their associated diffraction spots for a

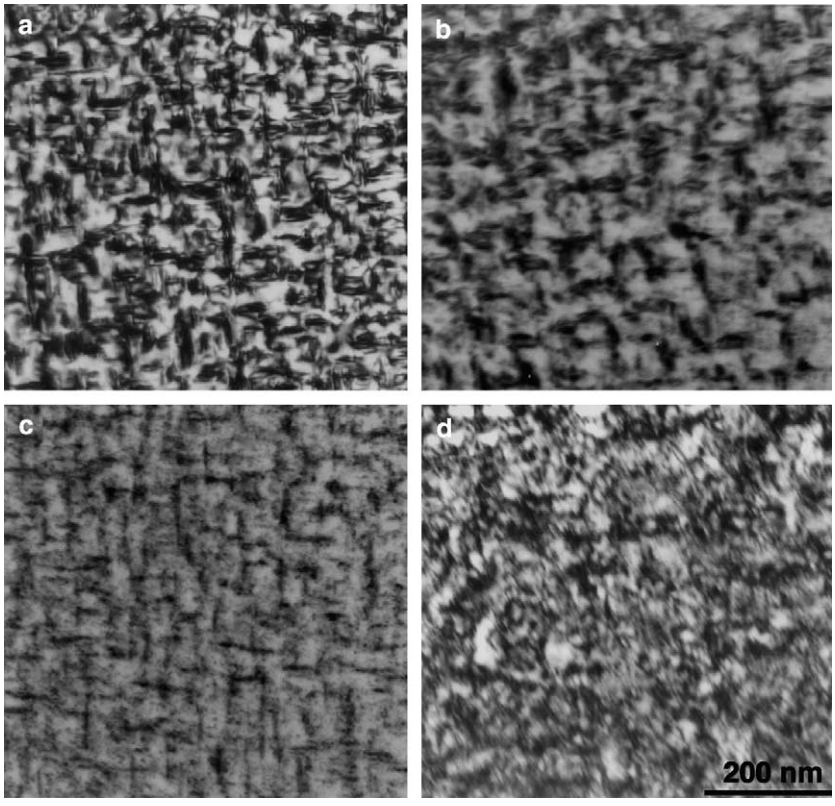

Fig. 7. Bright field TEM micrographs in the peak damage region of PH Inconel 718 irradiated by 3500 keV Fe-ions to (a) 0 dpa, (b) 0.1 dpa, (c) 1.0 dpa, and (d) 10 dpa.

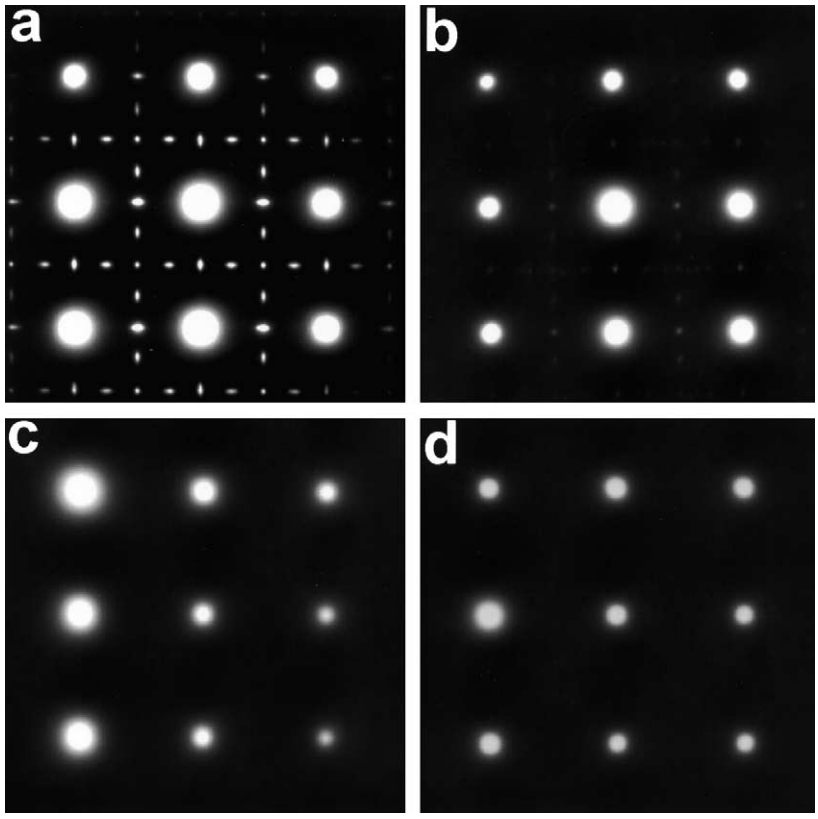

Fig. 8. Diffraction patterns taken along the [1 0 0] zone axis corresponding to the micrographs in Fig. 7 for PH Inconel 718 irradiated by 3500 keV Fe-ions to (a) 0 dpa, (b) 0.1 dpa, (c) 1.0 dpa, and (d) 10 dpa.

[1 0 0] orientation. By 0.1 dpa, the precipitates had begun to disappear and their diffraction spots became less intense. At 1 dpa, the diffraction spots for the γ' and γ'' precipitates were gone, although some residual contrast still remained in the bright field images. This may suggest that a structural homogenization was occurring while a compositional inhomogeneity between the matrix and post-precipitate zones still persisted. By 10 dpa, there was no further evidence of the precipitates. It is interesting to note that no rings appeared in the diffraction patterns associated with the break-up of the precipitates. That is, the γ' and γ'' precipitates did not become amorphous, but rather they dissolved back into solution.

After the γ' and γ'' precipitates dissolved, the softening in the irradiated layer was probably more dramatic than indicated by the nanoindentation measurement. The reason the nanoindenter was only able to measure a slight softening was due to the difficulty in sensing a thin soft layer sandwiched between two hard layers. This is a different situation than in the SA case, where the indenter is sensing a hard layer in a softer matrix, and care must be taken in comparing results for the two cases. During nanoindentation, a hard layer tends to mask an underlying soft layer more than when the situation is reversed [23–25]. This results in a greater sensitivity when attempting to measure radia-

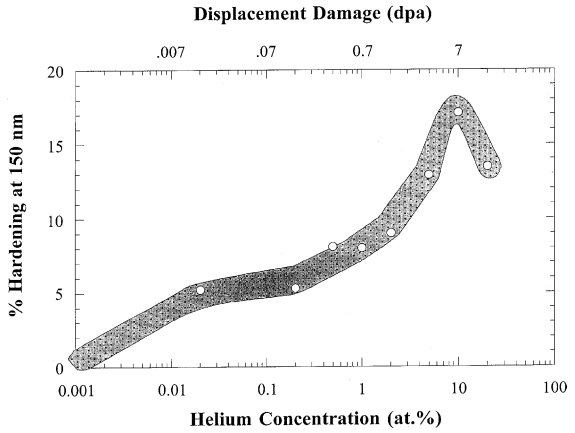

Fig. 9. Percent hardening at 150 nm contact depth, relative to the unirradiated material, for PH Inconel as a function of helium concentration from 370 keV He-injection. Upper axis shows the associated displacement damage caused by the He-ions.

tion-induced hardening of a buried layer compared to radiation-induced softening.

Fig. 9 shows the effect of He-ion injection into PH Inconel 718. A net hardening as a function of helium concentration was observed. In this case, the build-up of helium in the lattice and its associated deformation pinning occurred at a greater rate than the dissolution of the γ' and γ'' precipitates, given the relatively low displacement rate of the light He-ions. At 20 at.% He, which corresponded to 14 dpa, some reversal of the hardening was evident, probably due to precipitate dissolution.

4. Conclusion

Ion-irradiation-induced hardening in Inconel 718, both in the SA and the PH condition, has been studied using a nanoindentation technique. Specimens were irradiated to displacement doses ranging from 0.01 to 10 dpa by 3500 keV Fe-ions. The SA material showed a systematic hardening as a function of dose. Conversely, the PH Inconel exhibited a dose dependent softening caused by the radiation-induced dissolution of the γ' and γ'' precipitates. Specimens irradiated to the same displacement dose with a concomitant injection of 200 appm He/dpa and 1000 appm H/dpa showed no difference in the observed hardening as measured by the nanoindenter.

Irradiations were also performed with He-ions alone to concentrations as high as 20 at.%. SA Inconel 718 showed a hardening beyond what would arise from the He-induced displacement damage alone. Presumably due to helium bubble formation, as has been previously observed in 316LN stainless steel irradiated under the same conditions. PH Inconel also showed hardening as a function of helium concentration, demonstrating that the helium build-up was more effective in producing hardening than the He-induced displacement damage was in producing softening by dissolving the γ' and γ'' precipitates.

Acknowledgements

This research was sponsored by the Division of Materials Sciences an Engineering, US Department of Energy, under contract No DE-AC05-00OR22725 with UT-Battelle, LLC. We would like to thank S.W. Cook for assistance with irradiations and Drs M.B. Lewis and D.T. Hoelzer for technical review of the manuscript.

References

[1] J.D. Hunn, E.H. Lee, T.S. Byun, L.K. Mansur, J. Nucl. Mater. 282 (2000) 131.
[2] J.D. Hunn, M.B. Lewis, E.H. Lee, in: AccApp 98 – Second International Topical meeting on Nuclear Applications of Accelerator Technology, American Nuclear Society, La Grange Park, 1998, p. 375.
[3] E.H. Lee, G.R. Rao, J.D. Hunn, P.M. Rice, M.B. Lewis, S.W. Cook, K. Farrell, L.K. Mansur, in: M.S. Wechsler, L.K. Mansur, C.L. Snead, W.F. Sommer (Eds.), Materials for Spallation Neutron Sources, TMS, Warrendale, PA, 1998, p. 57.
[4] E.H. Lee, J.D. Hunn, N. Hashimoto, L.K. Mansur, J. Nucl. Mater. 278 (2000) 266.
[5] E.H. Lee, J.D. Hunn, T.S. Byun, L.K. Mansur, J. Nucl. Mater. 280 (2000) 18.
[6] E.H. Lee, J.D. Hunn, G.R. Rao, L.K. Mansur, J. Nucl. Mater. 272 (1999) 385.
[7] M.B. Lewis, W.R. Allen, R.A. Buhl, N.H. Packan, S.W. Cook, L.K. Mansur, Nucl. Instrum. and Meth. B 43 (1989) 243.
[8] L.K. Mansur, A.D. Brailsford, W.A. Coghlan, Acta Metall. 33 (1985) 1420.
[9] L.K. Mansur, M.H. Yoo, J. Nucl. Mater. 85&86 (1979) 529.
[10] J.F. Ziegler, J.P. Biersack, U. Littmark, The Stopping and Ranges of Ions in Solids, Pergamon, New York, 1985.
[11] M.J. Norgett, M.T. Robinson, I.M. Torrens, Nucl. Eng. Des. 33 (1975) 50.
[12] P. Wang, Y. Li, J. Liu, G. Zhang, R. Ma, P. Zhu, C. Qiu, T. Xu, J. Nucl. Mater. 169 (1989) 167.
[13] M.B. Lewis, K. Farrell, Nucl. Instrum. and Meth. B 16 (1986) 163.
[14] E.V. Kornelsen, Radiat. Eff. 18 (1972) 227.
[15] M.B. Lewis, J. Nucl. Mater. 149 (1987) 143.
[16] L.K. Mansur, J. Nucl. Mater. 216 (1994) 97.
[17] W.C. Oliver, G.M. Pharr, J. Mater. Res. 7 (1992) 1564.
[18] L.E. Samuels, T.O. Mulhearn, J. Mech. Phys. Solids 5 (1957) 125.
[19] J. Chen, Y. Dai, F. Carsughi, W.F. Sommer, G.S. Bauer, H. Ullmaier, J. Nucl. Mater. 275 (1999) 115.
[20] F. Carsughi, H. Derz, P. Ferguson, G. Pott, W. Sommer, H. Ullmaier, J. Nucl. Mater. 264 (1999) 78.
[21] W.L. Bell, T. Lauritzen, E.S. Darlin, R.W. Warner, in: Irradiation Effects on the Microstructure and Properties of Metals, ASTM STP 611, American Society of Testing and Materials, 1976, p. 353.
[22] B.H. Sencer, G.M. Bond, F.A. Garner, M.L. Hamilton, B.M. Oliver, L.E. Thomas, S.A. Maloy, W.F. Sommer, M.R. James, P.D. Ferguson, J. Nucl. Mater. 283 (2000) 324.
[23] J.C. Hay, G.M. Pharr, Mater. Res. Soc. Symp. Proc. 505 (1998) 65.
[24] G.M. Pharr, A. Bolshakov, T.Y. Tsui, J.C. Hay, Mater. Res. Soc. Symp. Proc. 505 (1998) 109.
[25] T.Y. Tsui, G.M. Pharr, J. Mater. Res. 14 (1999) 292.